Flow Turbulence Combust (2010) 85:735–761
DOI 10.1007/s10494-010-9298-8

Effect of Particle Clusters on Carrier Flow Turbulence: A Direct Numerical Simulation Study

Ying Xu · Shankar Subramaniam

Received: 4 February 2010 / Accepted: 1 September 2010 / Published online: 23 September 2010

Abstract Experiments indicate that particle clusters that form in fluidized–bed risers can enhance gas-phase velocity fluctuations. Direct numerical simulations (DNS) of turbulent flow past uniform and clustered configurations of fixed particle assemblies at the same solid volume fraction are performed to gain insight into particle clustering effects on gas-phase turbulence, and to guide model development. The DNS approach is based on a discrete-time, direct-forcing immersed boundary method (IBM) that imposes no-slip and no-penetration boundary conditions on each particle's surface. Results are reported for mean flow Reynolds number $Re_p = 50$ and the ratio of the particle diameter d_p to Kolmogorov scale is 5.5. The DNS confirm experimental observations that the clustered configurations enhance the level of fluid-phase turbulent kinetic energy (TKE) more than the uniform configurations, and this increase is found to arise from a lower dissipation rate in the clustered particle configuration. The simulations also reveal that the particle-fluid interaction results in significantly anisotropic fluid-phase turbulence, the source of which is traced to the anisotropic nature of the interphase TKE transfer and dissipation tensors. This study indicates that when particles are larger than the Kolmogorov scale ($d_p > \eta$), modeling the fluid-phase TKE alone may not be adequate to capture the underlying physics in multiphase turbulence because the Reynolds stress is anisotropic. It also shows that multiphase turbulence models should consider the effect of particle clustering in the dissipation model.

Keywords Direct numerical simulation · Turbulence · Particle clustering

Submitted for the Special Issue dedicated to S. B. Pope.

Y. Xu · S. Subramaniam (✉)
Department of Mechanical Engineering, Iowa State University, Ames, IA 50011, USA
e-mail: shankar@iastate.edu

Present Address:
Y. Xu
Shanghai Supercomputing Center, Shanghai, 201203, China

1 Introduction

Flows involving a carrier gas or liquid laden with solid particles are ubiquitous in industry. Gas-solid flows are important in conventional industrial processes such as fluidized–bed combustion, fluid catalytic cracking (FCC) and coal gasification. There is also renewed interest in studying these flows in the context of biomass energy generation [14, 34], and other emerging technologies such as chemical looping combustion for environmentally–friendly energy generation. One of the challenges in the development of these technologies is the design and scale-up of the components involving particle–laden flow. Fluidized beds and pneumatic transport lines where particle–laden flows are usually encountered are notoriously hard to design and scale up [29].

Device-scale calculations using computational fluid dynamics (CFD) of the averaged equations of multiphase flow are a promising route to inexpensive design and scale-up of industrial process equipment involving multiphase flows. It is expected that CFD will play an ever-increasing role in the design and scale-up of process equipment involving particle–laden flows [21]. CFD of multiphase flow involves solving the averaged equations in each phase [13, 26], which contain unclosed terms. The closure of these equations requires modeling of average stresses and second moments of the fluctuating velocity in both phases.

The focus of this work is on fluctuations in the fluid–phase velocity and their interaction with particle clusters. It is important to note that fluid velocity fluctuations in particle–laden flow also arise from the disturbance flow caused by the presence of particles and their evolving configuration, in addition to turbulent motions in the fluid phase. Therefore, even "laminar" particle–laden flows exhibit non–zero fluid velocity fluctuations. Current averaging procedures and most closure models do not distinguish between these two different physical mechanisms that give rise to fluid–phase velocity fluctuations, since both mechanisms essentially manifest themselves as a non–zero second moment of fluid velocity. The effects of particles on fluid phase turbulence have been studied experimentally (see e.g., [59]). Also CFD calculations of particle–laden flow [8] indicate that the model for interaction of gas–phase turbulence with particles affects the predicted mean velocity profiles. Although the second moment of fluid velocity is sometimes neglected in gas-solid flow on the grounds that the particle phase represents the major portion of the mixture momentum and energy, it is important to retain and model this term. Even though the second moment of fluid velocity may be small in comparison to the mixture energy, one cannot neglect the subgrid fluid motions in CFD calculations of gas-solid flow. The gas phase turbulence model effectively contributes an essential additional "eddy" viscosity to the viscous term in the mean fluid momentum equation. These gas–phase fluctuations also contribute to the generation of particle velocity fluctuations, that in turn influence mean flow structure in risers. Furthermore, the interaction of fluid–phase velocity fluctuations with particles, or clusters of particles, can enhance their magnitude.

Clustering of particles occurs in gas-solids suspensions in a volume fraction range from a few percent to about 30%. Particle clusters are observed as an inhomogeneous solid volume fraction profile in the radial direction inside the circulating fluidized bed, where a dilute gas-solid suspension preferentially moves upward in the core and

a dense annulus of particle clusters, or strands, moves downward along the wall [10]. Recently, particle clusters have been directly visualized using a borescope and a high-speed camera [12]. Thus, a variety of experiments using different techniques conclusively reveal that particles do form clusters in particle-laden suspension flow [7, 30, 71].

Clusters of particles with characteristic size on the order of $10d_p$–$100d_p$ [20] are found to significantly affect the overall flow behavior. It is worth noting that clusters of high–inertia particles (Stokes number $O(100)$) formed in fluidized beds and risers are different from the clustering of lower inertia particles (Stokes number $O(1-10)$) in turbulent flow [52]. While current CFD simulations of gas-solid flow are capable of reproducing the core-annulus flow in risers [9, 47, 48], there is still considerable uncertainty regarding models for gas-particle interaction. Phenomenological models of cluster drag have been proposed to explicitly account for the formation of clusters [22, 30, 41, 67], but these may not be predictive for general flows because they lack information about the microscale flow physics. Also to the best of our knowledge, the interaction between fluid-phase velocity fluctuations and particle clusters has not been modeled. This work aims to provide this much–needed insight into the microscale flow physics through particle–resolved direct numerical simulations (DNS) of turbulent flow past assemblies consisting of several particles.

Experiments by Moran and Glicksman [38] report gas–phase velocity fluctuations measured inside a circulating fluidized bed (CFB) at dilute particle concentrations ($\sim$1–5%). The measurements indicate that at larger particle concentrations where clusters usually form, the gas–phase velocity fluctuations increase dramatically. Moran and Glicksman [38] suggest that a length scale based on the particle cluster size, as opposed to the particle size, should be used to estimate the increased levels of gas–phase velocity fluctuations caused by the particle phase. It is worth noting that they interpret their experimental results using a criterion suggested by Gore and Crowe [19] to arrive at this inference. One of the principal findings of the Gore and Crowe [19] study is that fluid–phase turbulence intensity increases dramatically if $d_p/l_e > 0.1$, where d_p is the size of particle and l_e is characteristic length scale of the most energetic eddy in the flow. For d_p/l_e below this critical value 0.1, the presence of particles does not increase turbulence intensity. The ratio $d_p/l_e = 0.01$ in Glicksman's experiments is an order of magnitude below the cutoff value 0.1 suggested by Gore and Crowe [19] for turbulence enhancement due to particles. Therefore, the Gore and Crowe criterion indicates that the addition of small particles (164μm) would lead to a *decrease* in turbulence intensity in the Glicksman experiments. However, the experimental data show 158% increase of turbulence intensity inside the CFB. Moran and Glicksman attribute this discrepancy to the continuous formation and breakage of particle clusters in CFB. A plausible explanation advanced by Moran and Glicksman to describe the apparent increase in gas phase fluctuations is that the dominant structures are particle clusters, with the dominant particle length scale being the cluster size d_c, instead of the particle diameter d_p. If the length scale of the particle cluster d_c is chosen as the particle phase length scale in Gore and Crowe's criterion, then $d_c/l_e = 1.25$, which is an order of magnitude greater than the cutoff value of 0.1. Now applying the Gore and Crowe's criterion with d_c instead of d_p, Moran and Glicksman show that the fluid

phase TKE increases with the addition of particles as observed in their experiments. The difficulties in performing measurements in gas-solid flow pose a considerable challenge to obtaining direct evidence of this effect from such experiments.

The experimental findings of Moran and Glicksman [37, 38] suggest that turbulence models for gas-solid flows should incorporate a dependence on particle cluster size, but it is difficult to extract data from these experiments for modeling purposes. DNS offers an alternative means of investigating the effect of particle clustering in turbulent gas-solid flows. In principle, DNS can be used to directly quantify unclosed terms in Eulerian–Eulerian (EE) models [1, 2, 6, 54]. Using DNS to study the effects of particle clusters on the unclosed terms in EE models can provide valuable insight into fluid-phase TKE modulation by particle clusters.

DNS of particle–laden flow can be classified as those that resolve the flow around each particle, or "particle–resolved" DNS, and those that do not. The point-particle approximation is usually invoked in DNS that do not resolve the flow around each particle. This approximation is based on the assumption that the particle size is smaller than the Kolmogorov length scale of fluid-phase turbulence. If the particle size is comparable to (or larger than) the Kolmogorov scale, then particle–resolved DNS is the appropriate simulation approach. In Glicksman's experiment [38], they estimate the Kolmogorov scale η to be approximately 146μm. Since the particle diameter $d_p = 164\mu$m, a particle–resolved DNS approach is necessary because $d_p > \eta$.

Recently a variety of numerical approaches have been developed for particle–resolved direct numerical simulation. These can be broadly classified as those that rely on a body–fitted mesh to impose boundary conditions at particle surfaces, and those that employ regular Cartesian grids. The body-fitted methods include the arbitrary Lagrangian Eulerian (ALE) approach [25, 40] as well as the method used by Bagchi and Balachandar [4, 5]. Also Burton and Eaton [11] used the overset grid technique to study the interaction between a fixed particle and decaying homogeneous isotropic turbulence. The principal disadvantage with approaches based on body-fitted meshes is that repeated re-meshing and solution projection are required for moving interfaces. Even for fixed particle simulations the cost of meshing a single configuration can be significant, and for random assemblies it is necessary to simulate many such configurations to account for statistical variability.

For methods that employ regular Cartesian grids this need for re-meshing and projection is eliminated, resulting in much faster solution times for moving particle simulations and multiple random spatial configurations of fixed particle assemblies. However, because the grid does not conform to the particle surface, special attention is needed to generate an accurate solution. Prosperetti has developed a method called PHYSALIS that uses a general analytic solution of the Stokes equation in the flow domain close to particle boundaries to impose the no-slip velocity boundary condition on the particle surface [50, 56, 69, 70]. This method is numerically efficient and is shown to be accurate for flow over a single particle up to a Reynolds number of 100. One limitation of PHYSALIS is the need for an exact analytical solution of the Stokes equation, which only exists for a few body shapes. Also detailed comparison for multiparticle simulations is needed to validate the underlying assumptions for more general problems. Other methods based on regular Cartesian grids include the fictitious domain method, the Lattice Boltzmann method (LBM), and the immersed boundary method (IBM). The fictitious–domain method with Lagrange multipliers has been developed to solve flow past many moving particles by several research

groups [3, 16, 17, 44, 53]. LBM has been used to simulate flow through a fixed bed of spheres [23, 24, 62, 64] and for particulate flows [31, 32, 57]. IBM was proposed by Peskin [45, 46] to simulate flexible boundaries in a flow field. More recently, several researchers [15, 27, 35, 36, 60, 61] have modified IBM to study the interaction between flow and rigid particles. LBM simulation of turbulent liquid–solid suspensions by Ten Cate et al. [57], and IBM simulations by Uhlmann [60, 61] and Lucci et al. [35] are examples of particle–resolved DNS with multiple moving particles in turbulence.

Typically spectral methods have been used in DNS of single–phase turbulent flows because of their high accuracy, and the numerical method used in this work exploits a partially pseudo-spectral implementation for this reason. Finite–difference and finite–volume methods require sophisticated high-order schemes in order to simulate turbulence with numerical accuracy comparable to spectral methods [39, 63]. In flows where $d_p/\eta > 1$, the resolution requirement is dictated by the particle diameter rather than the Kolmogorov scale, and this may be less of an issue.

We use a discrete-time implementation of a direct-forcing immersed boundary approach on a regular Cartesian grid developed by Mohd. Yusof [36]. The dynamically changing resolution requirement is not an issue because we simulate flow over fairly dilute fixed particle assemblies where the resolution requirement is determined by the fixed particle configuration and the Reynolds number. The scaling of computational cost in IBM with number of particles is excellent because of the implicit imposition of boundary conditions through a forcing term in the Navier–Stokes equations. For example, going from 2 to 100 particles the computational cost increases by only 25%. The Fourier–Fourier-finite difference implementation of IBM [36] that is used in this work to simulate homogeneous particle assemblies exploits periodic boundary conditions in the cross-stream directions (the flow is statistically homogeneous in planes perpendicular to the mean flow direction) to achieve spectral accuracy in the cross-stream directions. The approach also reduces the Poisson pressure solution to a simple tridiagonal matrix system. Spectral accuracy in the IBM implementation is a significant advantage when simulating turbulent flow past particles. Therefore, we choose the IBM approach for simulating turbulent flow past fixed particle assemblies for the following reasons: (i) excellent scaling of computational cost with number of particles, (ii) spectral accuracy in cross-stream directions, and (iii) simplification of pressure solution for the statistically homogeneous problem to a tridiagonal matrix solution.

The objective of our study is to examine the effects of particle clustering on fluid–phase turbulence. Although the interaction of a single particle with turbulent flow has been studied by other researchers [4, 5, 11, 36], there are few particle–resolved DNS studies of turbulence interacting with several particles [57]. Even in these studies [57], the nature of how particle clusters affect fluid–phase turbulence is not addressed. Toward this end we use IBM as a particle–resolved DNS approach to simulate turbulent flow past a fixed bed of spheres. Fixed particle assemblies have been used as a reasonable approximation to a freely moving suspension of high Stokes number particles for extracting computational drag laws from DNS [15, 62, 64, 68]. We use the same approximation here to enable some additional simplifications specific to the particle clustering problem. By using fixed particle assemblies we can generate different particle configurations corresponding to clustered and uniform distributions, and maintain a constant pair correlation function throughout the

simulation.[1] In order to isolate the effect of clustering, we generate the uniform and clustered distributions at the same solid volume fraction. In this way we can quantify the effect of particle clustering on fluid turbulence with greater confidence than in a freely–evolving suspension where the level of clustering cannot be controlled. With stationary spheres we also avoid uncertainties associated with collision modeling and lubrication forces when spheres come close to each other.

Since the particle velocities change on the particle momentum response time scale, by defining a characteristic flow time scale as $20\,d_p/|\langle \mathbf{U} \rangle|$ we find that a Stokes number defined as the ratio of these two time scales characterizes the change of the velocity state of the particles. This Stokes number can be rewritten as $St = (1/18)(\rho_p/\rho_f)\,Re_p/20$, which informs us that for moderate particle Reynolds number $Re_p \sim O(10)$ and high density ratio of particles to fluid (e.g., for coal particles in air $\rho_p/\rho_f \sim 1{,}000$) results in relatively large particle Stokes number $O(100)$. This means that the particle velocity changes little over the time it takes for the flow turbulence to lose memory of its initial conditions. The other relevant timescale ratio is the time that the particle configuration takes to change compared to $d_p/|\langle \mathbf{U} \rangle|$, and this time scale ratio depends on $Re_T = d_p T^{1/2}/\nu$, which is the Reynolds number based on the particle fluctuating velocity that is characterized by the particle granular temperature T. In our simulations we have $Re_T = 0$. While one expects finite granular temperature in risers, both direct numerical simulations of freely–evolving suspensions [58] and recent high–speed imaging of particles [12] show that this value of Re_T is low. Hence, these numerical simulations of turbulence past fixed clusters of spheres can be considered a reasonable approximation to gas–solid riser flows where particles have high Stokes number (moderate Re_p, high particle/fluid density ratio) and relatively low levels of particle velocity fluctuations.

A notable difference between the turbulent case considered here and the simulation of steady nonturbulent flow past a homogeneous bed of fixed particles to extract mean drag laws [15, 62, 64, 68] is that the flow quantities in our setup are statistically inhomogeneous in the flow direction. In order to understand the modification of turbulence by particles, an initially homogeneous, isotropic turbulence field is convected with a specified mean flow velocity over a homogeneous bed of spheres (see Fig. 1). This is accomplished with inflow/outflow boundary conditions in the flow direction, whereas in the nonturbulent case it is customary to use periodic boundary conditions on the statistically homogeneous fluctuation fields. As a consequence, in this study the flow statistics change along the axial direction as the turbulence is progressively affected by interaction with the particles starting from its initial undisturbed state upstream of the bed. In this setup the flow statistics can vary along the axial flow direction, but the flow is statistically homogeneous in the cross-flow plane and reaches a statistically stationary state. This allows us to use time-averaging and spatial averaging over the cross-plane when computing axially varying flow statistics from the DNS data. An alternative approach would be to extract time–varying statistics from the decay of homogeneous particle-laden turbulence and

[1] The pair correlation function is a statistical measure of the level of particle clustering in a homogeneous system.

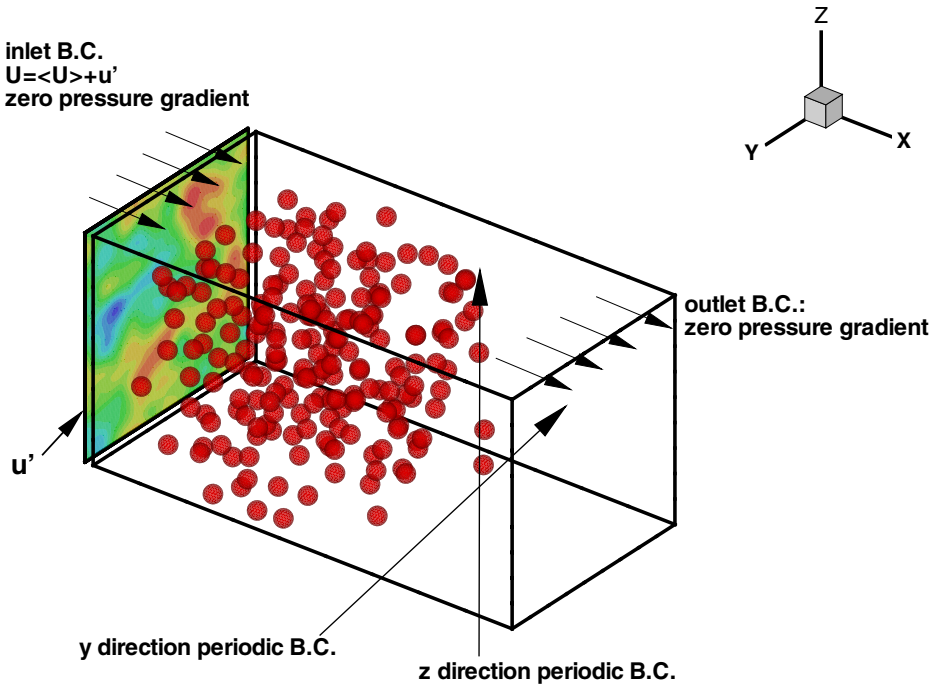

Fig. 1 The computational domain containing a statistically homogeneous assembly of randomly distributed particles. Periodic boundary conditions are imposed in the cross-stream y and z directions, and a zero pressure gradient boundary condition is imposed at the convective outflow boundary. Contours of the fluctuating velocity u' are shown at the zero pressure gradient inflow plane

compare the clustered and uniform cases, but the low levels of turbulence that can be simulated using particle–resolved DNS render this option less attractive.

The rest of the paper is organized as follows. In Section 2 the simulation methodology including the DNS approach is described, and validation results are presented. The test problems chosen to characterize the effect of uniform and clustered particle configurations on turbulent flow, and the DNS results for these cases are described in Section 3. The implications of the DNS results for multiphase turbulence modeling are discussed in Section 4, and conclusions are drawn in Section 5.

2 Simulation Methodology

The governing equations of the discrete-time, direct-forcing immersed boundary method (IBM) are described in Section 2.1 along with the boundary and initial conditions for turbulent flow past homogeneous fixed particle assemblies. This is followed by a brief description of the Fourier–Fourier-finite difference numerical scheme that is used to solve the governing equations. Salient features of the parallel implementation that is needed to solve the turbulent cases are summarized. Initialization of the particle configurations for the uniformly distributed and clustered cases is described. The approach used to generate the inflow turbulence field is outlined.

Numerical resolution requirements for the turbulent flow cases are discussed, and a feasible range of parameters is established based on these requirements. Validation of the simulations with existing results on turbulent flow past a single particle concludes this section.

2.1 Governing equations

We solve incompressible flow past a homogeneous assembly of fixed particles in a computational domain as shown in Fig. 1. The fluid velocity and pressure fields evolve by the incompressible Navier–Stokes equations from a specified initial state, subject to no–slip and no–penetration boundary conditions at the particle surfaces. For simplicity, the mean flow is taken to be along the positive x-direction, and so inflow/outflow boundary conditions are imposed on the boundary planes normal to the x-axis. Periodic boundary conditions are imposed in the cross-stream (y and z) directions.

The immersed boundary method [18, 36, 45] has the ability to handle moving or deforming bodies with complex surface geometry without body-fitted meshes. This enables the computation of flow past multiple particles with no-slip and no-penetration boundary conditions on uniform three-dimensional Cartesian grids. In our simulations we impose no–slip and no–penetration boundary conditions at particle surfaces by using the discrete-time, direct-forcing version of the immersed boundary method proposed by Mohd. Yusof [36]. In this approach the instantaneous velocity $\mathbf{u}(\mathbf{x}, t)$ and pressure $P(\mathbf{x}, t)$ fields evolve by

$$\frac{\partial \mathbf{u}}{\partial t} + (\mathbf{u} \cdot \nabla)\,\mathbf{u} = -\frac{1}{\rho}\nabla P + \nu \nabla^2 \mathbf{u} + \mathbf{f} \tag{1}$$

$$-\frac{1}{\rho}\nabla^2 P = \nabla \cdot ((\mathbf{u} \cdot \nabla)\mathbf{u} - \mathbf{f}) \tag{2}$$

where ρ is the fluid–phase density and ν is the fluid–phase kinematic viscosity. The forcing term $\mathbf{f}$ in the momentum equation is used to impose no-slip and no-penetration boundary conditions at the surface of each particle. Since this study considers stationary particles, the velocity at each particle surface is set to zero. The initial condition for this problem is steady nonturbulent flow past the particle assembly.

Following Mohd. Yusof [36], the governing equations are partially Fourier transformed in the y- and z- directions to obtain the following evolution equations:

$$\frac{\partial \tilde{u}}{\partial t} + \tilde{S}_x = -\frac{1}{\rho}\frac{\partial \tilde{P}}{\partial x} + \nu \frac{\partial^2 \tilde{u}}{\partial x^2} - \nu\left(\kappa_y^2 + \kappa_z^2\right)\tilde{u}, \tag{3}$$

$$\frac{\partial \tilde{v}}{\partial t} + \tilde{S}_y = -\frac{1}{\rho}\iota\kappa_y \tilde{P} + \nu \frac{\partial^2 \tilde{v}}{\partial x^2} - \nu\left(\kappa_y^2 + \kappa_z^2\right)\tilde{v}, \tag{4}$$

$$\frac{\partial \tilde{w}}{\partial t} + \tilde{S}_z = -\frac{1}{\rho}\iota\kappa_z \tilde{P} + \nu \frac{\partial^2 \tilde{w}}{\partial x^2} - \nu\left(\kappa_y^2 + \kappa_z^2\right)\tilde{w}, \tag{5}$$

where $\tilde{u}$, $\tilde{v}$, $\tilde{w}$ and $\tilde{P}$ are the partially Fourier transformed fields in $(x, \kappa_y, \kappa_z, t)$ space. In (3)–(5) the nonlinear terms $\tilde{S}_x$, $\tilde{S}_y$ and $\tilde{S}_z$ are given by

$$\tilde{S}_x = \mathscr{F}\left(\frac{\partial uu}{\partial x} + \frac{\partial uv}{\partial y} + \frac{\partial uw}{\partial z}\right), \tag{6}$$

$$\tilde{S}_y = \mathscr{F}\left(\frac{\partial vu}{\partial x} + \frac{\partial vv}{\partial y} + \frac{\partial vw}{\partial z}\right), \tag{7}$$

$$\tilde{S}_z = \mathscr{F}\left(\frac{\partial wu}{\partial x} + \frac{\partial wv}{\partial y} + \frac{\partial ww}{\partial z}\right), \tag{8}$$

where $\mathscr{F}$ represents the two–dimensional, spatial Fourier transform from (x, y, z, t) to $(x, \kappa_y, \kappa_z, t)$ space. The pressure Poisson equation in (2) becomes

$$-\frac{1}{\rho}\left(\frac{\partial^2 \tilde{P}}{\partial x^2} - \left(\kappa_y^2 + \kappa_z^2\right)\tilde{P}\right) = \frac{\partial \tilde{S}_x}{\partial x} + \iota\kappa_y \tilde{S}_y + \iota\kappa_z \tilde{S}_z - \left(\frac{\partial \tilde{f}_x}{\partial x} + \iota\kappa_y \tilde{f}_y + \iota\kappa_z \tilde{f}_z\right) \tag{9}$$

where $\iota = \sqrt{-1}$.

The numerical scheme [36, 65] that is used to solve (3)–(9) is a primitive-variable, pseudo-spectral method, using fast Fourier transforms in the y- and z- directions, and centered finite differences in the x- (streamwise) direction. The fractional time-stepping scheme proposed by Kim and Moin [28] is used to advance the velocity field in time. The Adams-Bashforth scheme is used for the nonlinear terms in (6)–(8), and the Crank–Nicolson scheme is used for the diffusion terms.

This approach was used by Mohd. Yusof [36] to simulate turbulent flow past a single sphere. Subsequently, improvements to this approach were implemented in a new code that was developed by Xu [65], which was extensively tested and validated. Selected validation test results are presented later in this section. As shown later in this section, the choice of parameters dictated by numerical resolution requirements for turbulent flow past several particles requires parallelization of the IBM DNS code. The advantage of the IBM approach is that it enables the use of Cartesian grids, which considerably simplifies parallelization of the solver as compared to unstructured body-fitted grids. Using domain decomposition, the grid is partitioned among processors and the numerical solver is parallelized on computer clusters with distributed memory [65]. For this study a serial implementation of Mohd. Yusof [36]'s IBM approach is parallelized to achieve this objective. Details of the parallelization can be found in Xu [65].

2.2 Particle initialization

The particle centers in the fixed bed are generated to correspond to two cases with different levels of clustering at the same average solid volume fraction: (a) a near-uniform distribution of particles, and (b) a clustered distribution of particles (see inset of Fig. 2). All the particles are spherical and of the same size. The near-uniform distribution of non-overlapping spheres is generated using the Matérn hard-core point process [55]. This is essentially a Poisson point process for particle centers from which overlapping spheres have been removed using an approach called dependent

thinning. The Matérn hard-core point process results in particles homogeneously distributed in a volume with minimum particle clustering effects. It has an analytic form for the pair correlation function that is plotted in Fig. 2.

To generate clustered distributions of particles we choose the particle centers from homogeneous granular gas simulations [42]. These particle clusters are assumed to be representative of those found fluidized beds and risers, which are qualitatively different from particle clusters observed in particle-turbulence studies. In these hard–sphere molecular dynamics simulations, particles form clusters by interacting through inelastic collisions from a specified initial equilibrium state. To attain this initial equilibrium state, particle positions are specified according to a Matérn hard-core point process as described in Stoyan et al. [55] and the particle velocity distribution is initialized to be Maxwellian. Then each particle undergoes at least 100 elastic collisions at which point the particle configuration and temperature have reached equilibrium. From this equilibrium initial condition the particles now evolve under inelastic collisions with the normal coefficient of restitution set to 0.5 in these simulations. Under the influence of inelastic collisions the particle granular temperature decays, and the system is denoted a granular cooling gas.

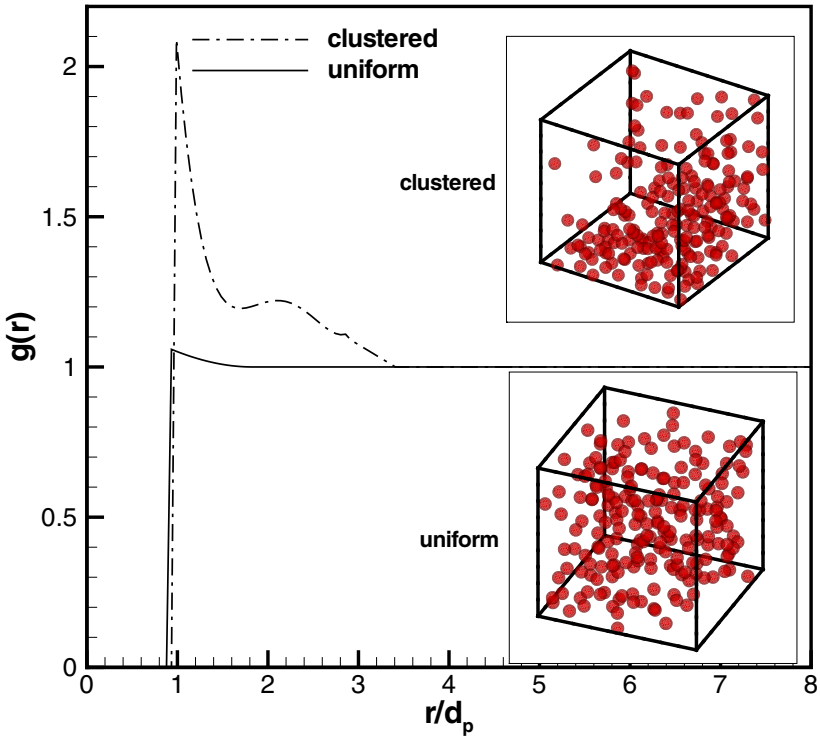

Fig. 2 The pair correlation function $g(r)$ for the uniformly distributed and clustered particle configurations. The *solid line* is the analytical form of the pair correlation for the Matérn hard-core distribution [55]. The *dash-dot line* represents the pair correlation for the clustered state of inelastic granular cooling gas obtained from hard-sphere MD calculations

In the homogeneous cooling state, the energy in the system decays according to Haff's cooling law. Beyond the homogeneous cooling state (HCS), the granular system develops clusters. The particle positions are chosen from the granular gas simulation at a simulation time of $10^4\tau$ (where $\tau = t\nu(0)$, and $\nu(0)$ is the Enskog collision frequency at initial time), which corresponds to a time instant well beyond the HCS and deep into the clustering regime. The level of the particle clustering can be characterized by the pair correlation function $g(r)$ (shown in Fig. 2), where r is the spatial separation between particle centers. These clustered configurations of particles from the granular gas simulations are used to then perform IBM DNS simulations of turbulent flow past fixed particle assemblies. Since the particles are fixed, the same level of clustering is maintained throughout the IBM DNS simulations, allowing us to quantify the effect of clustering on gas-phase velocity fluctuations.

2.3 Upstream turbulence initialization

To simulate upstream turbulence, velocity fluctuations are imposed at the inlet. The velocity field $\mathbf{U}$ is decomposed as $\mathbf{U} = \langle \mathbf{U} \rangle + \mathbf{u}'$, where $\langle \mathbf{U} \rangle$ is the mean velocity field and $\mathbf{u}'$ is the turbulent fluctuation. The upstream fluctuations $\mathbf{u}'$ are initialized as homogeneous, isotropic box turbulence using the classic algorithm by Rogallo [51], while the energy spectrum follows the model spectrum given by Pope [49]. This homogeneous, isotropic box turbulence is progressively convected into the computational domain by the inlet mean velocity $\langle \mathbf{U} \rangle$, where it then interacts with the fixed bed of particles. The simulation setup is shown in Fig. 1.

2.4 Numerical resolution requirements

Particle–resolved DNS of turbulent gas–solid flow must resolve all flow length and time scales. This imposes computational limitations on the range of parameters that can be simulated using particle–resolved DNS. In DNS of single-phase turbulence using a regular three-dimensional Cartesian grid of length $\mathscr{L}$ with N nodes in each direction, the limitations on the accessible range of parameters that are imposed by this resolution requirement [49] can be expressed as the scaling of the number of nodes N with Reynolds number:

$$N = \frac{\mathscr{L}}{\Delta x} = \left(\frac{\mathscr{L}}{L_{11}}\right)\left(\frac{L_{11}}{L}\right)\left(\frac{L}{\eta}\right)\left(\frac{\eta}{\Delta x}\right) \sim 1.6\left(\frac{L}{\eta}\right) = 1.6 Re_L^{3/4} = 0.4 R_\lambda^{3/2}, \quad (10)$$

where $Re_L = k_f^{1/2} L/\nu$ (with $L = k_f^{3/2}/\varepsilon$) is the turbulence Reynolds number, $R_\lambda = u'\lambda_g/\nu$ is the Taylor-scale Reynolds number, L_{11} is the longitudinal integral length scale, and η is the Kolmogorov length scale that must be resolved by the grid spacing $\Delta x = \mathscr{L}/N$. This estimate is valid for high Reynolds number turbulence where the ratio of L_{11} to L is constant ($L_{11}/L \approx 0.43$). In this case, the requirement that the computational box $\mathscr{L}$ be large enough to contain the energy–containing motions (that are estimated to be equal to L_{11}), can be expressed in terms of the ratio $\mathscr{L}/L$. Thus, the requirement in (10) can be interpreted as a combination of the resolution

requirement for the large scale motions expressed by the ratio $\mathscr{L}/L$ (taken to be 8×0.43 in (10)), and the resolution requirement for the small scale motions $\eta/\Delta x$ (taken to be $1.5/\pi$). These requirements are related by the ratio of large to small scale turbulent motions L/η that characterizes the dynamic range of turbulence. Therefore, for a given problem size N^3 that is determined by available computational resources, there is an upper limit to the Reynolds number that can be simulated.

Here we develop similar numerical resolution requirements for particle–resolved DNS of turbulent gas-solid flow that allow us to determine the accessible range of parameters. For this we must take into consideration the particle length scales in addition to the turbulence scales. Even the introduction of fixed particles requires the consideration of two important particle length scales: one is the particle diameter d_p, and the other is the characteristic length scale of the interstices between the particles d_I through which the fluid flows.

In order to resolve the length scales of the particle–induced flow field, the grid spacing Δx should be smaller than the boundary layer thickness δ. The boundary layer thickness δ around each particle is estimated to be $\delta/d_p \sim 1/\sqrt{Re_p}$, where $Re_p = |\langle \mathbf{U} \rangle| d_p/\nu$ and d_p is the particle diameter. This requirement imposes a restriction on Re_p, which is the Reynolds number based on mean slip velocity. Depending on the choice of mean flow Reynolds number and turbulence Reynolds number, the resolution of the particle boundary layer δ or the Kolmogorov scale η can be limiting. For the case considered in this paper, with particles larger than the Kolmogorov scale, and at sufficiently high mean flow Reynolds number $Re_p = 50$, the small scale resolution requirement is determined by the boundary layer resolution. If the boundary layer is resolved for these large particles, the Kolmogorov scale is in fact over-resolved when compared to single–phase DNS.

The limitation on the largest turbulent motions that can be represented in a DNS of single-phase turbulence in a computational domain of size $\mathscr{L}$ arises from requirement that the velocity autocorrelation should decay to zero within the domain [49]. If this criterion is violated, then imposing periodic boundary conditions at the boundaries results in unphysical effects in the simulations. Similar criteria need to be developed for turbulent particle-laden flows. For particle-laden flows, the same criterion when extended to the particle phase requires that the autocorrelation of particle force decay to zero within the domain. For fixed particle assemblies, the particle force autocorrelation is closely tied to the pair correlation function, and since that is constant and decays to unity within 4 particle diameters (cf. Fig. 2) we do not explicitly include this criterion in our estimation of the accessible parameter regime. Since we do not have any a priori estimates for the fluid velocity autocorrelation in particle–resolved DNS of gas-solid flow, we base our initial estimates from single–phase turbulent flow. Therefore, for the particular case considered in this paper, the resolution requirement at large scales is taken to be the same as that in single-phase turbulent flow.

Based on these small and large scale resolution requirements, we now estimate the scaling of the number of grid points N in each direction with the physical parameters of turbulent gas-solid flow. We express N using the small scale resolution requirement that the boundary layer around the particles be resolved as

$$N = \frac{\mathscr{L}}{\Delta x} = \left(\frac{\mathscr{L}}{L_{11}}\right)\left(\frac{L_{11}}{L}\right)\left(\frac{L}{\eta}\right)\left(\frac{\eta}{d_p}\right)\left(\frac{d_p}{\delta}\right)\left(\frac{\delta}{\Delta x}\right) \tag{11}$$

where again $L/\eta \sim Re_L^{3/4} \sim R_\lambda^{3/2}$, and $d_p/\delta \sim \sqrt{Re_p}$. For fixed resolution requirements of large scales ($\mathscr{L}/L_{11}$) and small scales ($\delta/\Delta x$), and fixed length scale ratios L_{11}/L and η/d_p, the remaining ratios can be expressed in terms of physical parameters. The scaling in terms of the mean flow Reynolds number Re_p and the Taylor–scale Reynolds number of upstream turbulence R_λ is

$$N \sim \left(\frac{\mathscr{L}}{L_{11}}\right)\left(\frac{L_{11}}{L}\right) R_\lambda^{3/2} \left(\frac{\eta}{d_p}\right) \sqrt{Re_p}\,\frac{\delta}{\Delta x} \sim R_\lambda^{3/2}\sqrt{Re_p}.$$

This scaling informs us that the cost to perform particle–resolved DNS of turbulent particle–laden flows is more expensive than that of single–phase DNS by a factor $\sqrt{Re_p}$. Therefore, for the same number of grid nodes the accessible values of R_λ will be correspondingly lower as the mean flow Reynolds number is increased.

Based on available computational resources we performed the DNS calculations on a $512 \times 256 \times 256$ grid. The first half (256^3) of the computational grid is initialized with box turbulence that is convected over the computational test section containing the fixed particle assembly that occupies the second half of the grid. The mean flow Reynolds number Re_p is chosen to be 50, resulting in $\delta \sim d_p/7$ that requires $\Delta x < d_p/15$ to resolve the boundary layer. The important physical and numerical parameters in this DNS are listed in Table 1, where α_p denotes the volume fraction of solid particles, $u'/|\mathbf{V}|$ is the turbulence intensity, and where $\kappa_{\max}$ is the maximum wavenumber corresponding to the grid. As Table 1 shows, with $d_p/\Delta x = 20$ the ratio $\delta/\Delta x \approx 3$. Elsewhere Garg et al. [15] have shown that this resolution was adequate to obtain grid–converged results for the mean fluid–particle drag in steady nonturbulent flow past fixed assemblies of particles using a slightly different triperiodic implementation of IBM. Furthermore, for every realization of the particle configuration simulated in this study, it is guaranteed that there are at least two grid points between the nearest particle surfaces.

The turbulence intensity $u'/|\langle\mathbf{U}\rangle|$ encountered in fluidized beds is usually less than 40% [37, 38]. We choose the turbulence intensity to be 20% and the ratio of particle diameter to Kolmogorov scale $d_p/\eta = 5.55$. Therefore, the Kolmogorov scale η is guaranteed to be resolved as $\kappa_{\max}\eta = 11.3$. Note that the suggested $\kappa_{\max}\eta$ value is 1.5 for single phase turbulence [49]. The relevant length scale ratio at the large scale that appears in (11) is $\mathscr{L}/L = 7.12$. The computational box length $\mathscr{L}$ is $12.8d_p$, indicating that the box is 3 times larger than the pair correlation length scale for the clustered particle configuration (cf. Fig. 2).

The time step Δt is chosen as follows

$$\Delta t = \nu \frac{\Delta x}{|\mathbf{U}| + \sqrt{\frac{2}{3}k_f}} \tag{12}$$

where ν is the Courant number. This is simply the CFL condition with the magnitude of instantaneous slip velocity rather than the magnitude of the mean slip velocity. After the flow has evolved for 1.5 flow–through times ($\mathscr{L}/|\langle\mathbf{U}\rangle|$) from the initial

Table 1 Parameters for simulation of turbulent flow past a fixed bed of spheres

α_p	$u'/\|\mathbf{V}\|$	ν	Re_p	d_p/η	R_λ	$d_p/\Delta x$	$\kappa_{\max}\eta$	$\mathscr{L}/\Delta x$
5%	20%	0.002	50	5.55	11.9	20	11.3	256

Table 2 Time averaged C_D from the parallelized IBM DNS solver is compared with the drag force coefficient reported by Bagchi and Balachandar [4]

$\langle Re_p \rangle$	$I = u_{rms}/\lvert \mathbf{V}_r \rvert$ (%)	C_D (IBM DNS)	C_D [4]
107	10	1.02	1.07
114	25	1.025	1.03
58	20	1.52	1.53

condition, if the instantaneous total kinetic energy of the fluid–phase in the computational test section changes by less than 1% over one flow–through time, the flow is deemed to have reached steady state. All the statistics reported in Section 3 are gathered after the flow field reaches this steady state.

2.5 Validation

DNS results using a parallel implementation of the immersed boundary method solver are validated in the test case of turbulent flow past a single particle. As noted earlier, the nonturbulent cases have been extensively validated elsewhere [15]. In Table 2 the mean drag coefficient for turbulent flow past a single particle obtained from the parallel IBM DNS on regular Cartesian grids is compared with the simulation results reported by Bagchi and Balachandar [4], which were performed on body-fitted spherical coordinate grids. We find reasonably good agreement for the mean drag coefficient at different mean flow Reynolds numbers and different levels of upstream turbulence intensity.

When comparing these simulations it should be noted that there are differences in the initialization of turbulence that could contribute to the small discrepancy in the mean drag values. In Bagchi and Balachandar [4] the turbulence field is a precomputed 256^3 DNS solution [33] that determines the energy spectrum and the microscale Reynolds number. In our simulations the turbulence field is initialized according to a model spectrum due to Pope [49]. Having validated the parallel IBM DNS solver for turbulent gas-solid flow, we now use it to investigate the effect of particle clustering on upstream turbulence.

3 Results

DNS results for turbulent flow past fixed particle assemblies in uniform and clustered configurations at the same solid volume fraction are reported. The uniform and clustered particle configurations are studied as two different cases in the numerical simulation. The uniform configuration is generated using the Matérn hard-core point process [55], while the clustered particle configuration is from particle centers of the granular gas simulation [42]. The flow field simulation setup is exactly the same for both cases. For each case four independent simulations are performed and the fluid phase turbulence statistics are estimated using ensemble-averaging method.

The parameters of the physical problem and the numerical parameters used in the simulation are listed in Table 1. The solid volume fraction is chosen to be 5%, which is characteristic of riser flows. It is also the maximum volume fraction for which measurements were reported by Moran and Glicksman [38], and the volume

fraction at which they conclude the effects of particle clustering on turbulence are most pronounced.

As noted earlier, the flow is statistically inhomogeneous in the axial direction. Therefore, in each DNS realization the flow statistics are functions of the axial coordinate x and are computed by averaging over the cross-plane after statistical stationarity has been attained. Multiple independent simulations (MIS) are performed for each of the two random arrangements (uniform particle configuration and clustered particle configuration) to capture the statistical variability arising from particle configurational effects. For both types of random particle arrangement—uniform and clustered—the flow statistics from each DNS realization corresponding to that arrangement are ensemble–averaged over the MIS, as detailed in Xu [65]. Due to computational limitations, only four MIS could be performed for each of the clustered and uniform cases.

3.1 Mean momentum balance in the fixed bed

Before looking at fluid-phase turbulence statistics, it is instructive to first understand the steady mean momentum balance in the fixed bed. From the inlet at $x = 0$ to $x \sim 2.5d_p$ (see Fig. 1) there is an "entrance region" where the flow adjusts to the particles in the bed. Although the flow is statistically inhomogeneous in the flow direction, beyond the entrance region the mean flow inside the fixed bed closely resembles the mean flow obtained by imposing a constant mean pressure gradient on flow past a homogeneous fixed assembly of particles with periodic boundary conditions. In other words, the mean fluid velocity attains a nearly constant value, resulting in a constant mean slip velocity. The mean velocity shows less than 5% variation in the "fully-developed" region of the bed, as shown in Fig. 3a. These variations are due to

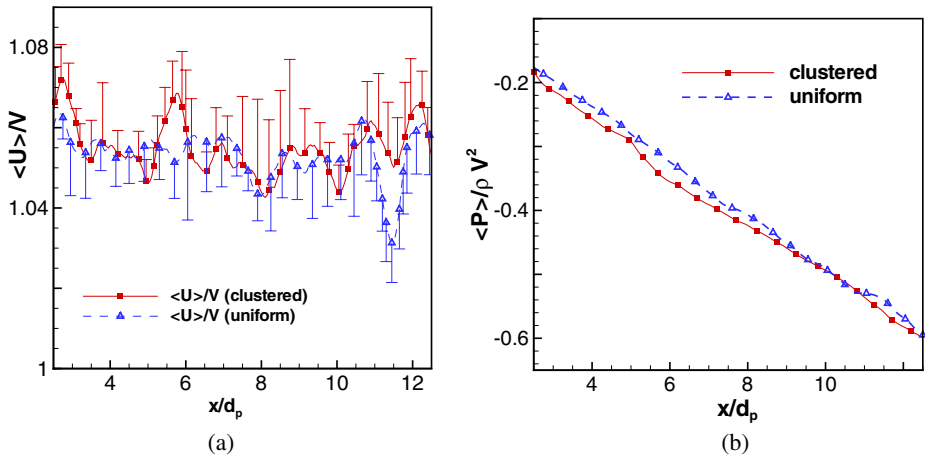

Fig. 3 Mean fluid velocity and mean pressure in the fully–developed region of the fixed bed. (**a**) The mean fluid velocity is nearly constant, resulting in a constant slip velocity. The variation in the mean fluid velocity $\langle U \rangle$ normalized by its reference upstream value V is less than 5% in the fully–developed region of the bed. The *error bars* represent the standard deviation in the ensemble–averaged mean. (**b**) Mean pressure decreases linearly resulting in an approximately constant pressure gradient in the fully–developed region of the fixed bed

the small number of independent realizations that could be performed, but it is clear that in the limit of infinite realizations the mean fluid velocity would be constant. The mean pressure decreases almost linearly (see Fig. 3b), resulting in a constant mean pressure gradient that balances the mean drag due to the presence of particles.

3.2 Turbulent kinetic energy inside the fixed bed

Figure 4 shows that the level of fluid phase TKE k_f inside the bed is enhanced relative to its upstream reference value by both the clustered and uniform particle configurations. The physical explanation for the enhancement of turbulence is the interaction of turbulence with particle wakes, and this has been noted by other studies on a single particle interacting with turbulence [36]. Beyond the entrance region ($x > 2.5d_p$), k_f in the clustered configuration is always higher than k_f for the uniform configuration. While k_f for the uniform particle configuration remains relatively unchanged as x increases inside the fixed bed, the clustered configuration appears to show an increase with x. It is implausible that this increase would continue indefinitely as the bed length is increased, so we conclude that a continued increase of fluid phase TKE along the flow direction is unphysical. It is expected that k_f in the clustered particle configuration will become independent of x if the computational domain is sufficiently long.

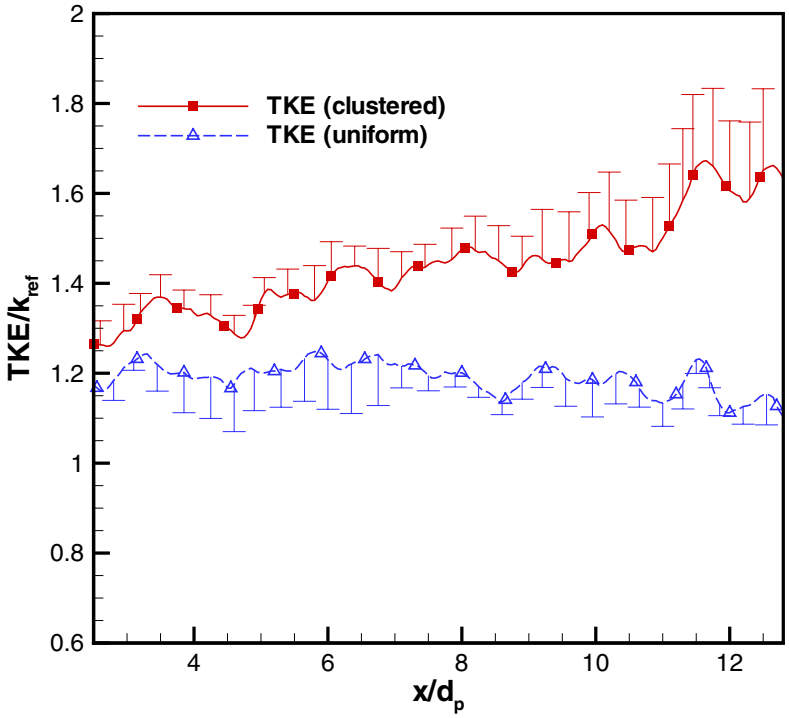

Fig. 4 Comparison of $k_f(x)$ normalized by its upstream value k_{ref} for uniform and clustered particle configurations. Particle clustering enhances gas-phase turbulence. *Error bars* in the plot indicate the standard deviation of $k_f(x)$ obtained from four different realizations

As noted earlier, the experiments performed by Moran and Glicksman [38] measure gas-phase velocity fluctuations for particle concentrations in the range ∼1–5% in a circulating fluidized bed (CFB). Their results indicate that gas-phase velocity fluctuations increase dramatically at higher particle concentrations where clusters are usually formed. This experimental result is inferred from the fact that higher gas-phase velocity fluctuations are found at higher particle concentrations. However, the level of particle clustering was not directly measured in these experiments. Our DNS results at 5% volume fraction shown in Fig. 4 confirm that increased fluid-phase fluctuations are found in the clustered particle configuration relative to the uniform configuration. The error bars in Fig. 4 show the standard deviation in k_f calculated from four independent simulations. Although the standard deviation of fluid-phase TKE k_f in the clustered particle configuration is considerably higher than that in the uniform case, it is still clear that the effects of particle clustering on gas-phase turbulence are statistically significant. On this basis we conclude that these DNS results show that the presence of particle clusters enhances fluid–phase velocity fluctuations, which supports the hypothesis of Moran and Glicksman [38]. However, due to computational limitations only a small set of realizations was feasible and a complete parametric study in volume fraction, mean flow Reynolds number and turbulence intensity space is outside the scope of this work.

3.3 Evolution of Reynolds stress in the fluid phase

In order to understand the enhancement of TKE in the fixed bed it is useful to examine the transport equation for the fluid phase TKE. Since k_f is half of the trace of the fluid-phase Reynolds stress, we examine the transport equation for $R_{ij}^{(f)}$, which is [43, 66]:

$$\begin{aligned}\langle I_f\rho_f\rangle\left[\frac{\partial}{\partial t}+\left\langle U_k^{(f)}\right\rangle\frac{\partial}{\partial x_k}\right]R_{ij}^{(f)} = &\underbrace{-\frac{\partial}{\partial x_k}\left\langle I_f\rho u_i^{\prime\prime(f)}u_j^{\prime\prime(f)}u_k^{\prime\prime(f)}\right\rangle}_{1}\\ &\underbrace{-\left\langle I_f\rho u_i^{\prime\prime(f)}\rho u_k^{\prime\prime(f)}\right\rangle\frac{\partial\left\langle U_j^{(f)}\right\rangle}{\partial x_k}-\left\langle I_f\rho u_j^{\prime\prime(f)}\rho u_k^{\prime\prime(f)}\right\rangle\frac{\partial\left\langle U_i^{(f)}\right\rangle}{\partial x_k}}_{2}\\ &+\underbrace{\left\langle u_i^{\prime\prime(f)}\frac{\partial(I_f\tau_{kj})}{\partial x_k}\right\rangle+\left\langle u_j^{\prime\prime(f)}\frac{\partial(I_f\tau_{ki})}{\partial x_k}\right\rangle}_{3}\\ &+\underbrace{\left\langle u_i^{\prime\prime(f)}M_j^{(f)}\right\rangle+\left\langle u_j^{\prime\prime(f)}M_i^{(f)}\right\rangle}_{4}\end{aligned}\tag{13}$$

The Reynolds stress in the fluid phase $R_{ij}^{(f)}$ evolves due to the following terms:

(1) the first term on the right hand side (denoted "1") is the transport of triple velocity correlations, with $u_i^{\prime\prime(f)}$ being the fluctuating velocity of the fluid phase;
(2) terms grouped as 2 correspond to the production $\mathscr{P}_{ij}$ due to mean flow gradient $\partial\langle U_i^{(f)}\rangle/\partial x_k$, where $\langle U_i^{(f)}\rangle$ is the mean fluid–phase velocity;

(3) terms grouped as 3 correspond to the fluctuating velocity–stress divergence correlations that result in dissipation;
(4) terms grouped as 4 correspond to interphase TKE transfer arising from fluctuating velocity–interfacial force correlations [43, 66], where $M_i^{(f)}$ is the interphase momentum transfer on the fluid side of the interface, and is given by $\tau_{ji} n_j^{(f)} \delta(\mathbf{x} - \mathbf{x}^{(I)})$. Here τ_{ji} is the stress tensor on the fluid side of the interface, $n_j^{(f)}$ is the unit normal at the interface pointing outward with respect to the fluid phase, and $\delta(\mathbf{x} - \mathbf{x}^{(I)})$ represents a generalized delta function located at the interface.

The fluctuating velocity–stress divergence tensor (grouped as 3 in (13)) is decomposed as $\Pi_{ij} + \Theta_{ij}$, corresponding to the contributions from pressure and viscous contributions to the stress tensor, where Π_{ij} is defined as

$$\Pi_{ij} \equiv -\left\langle u_i''^{(f)} \frac{\partial \left(I_f p''^{(f)}\right)}{\partial x_j} \right\rangle - \left\langle u_j''^{(f)} \frac{\partial \left(I_f p''^{(f)}\right)}{\partial x_i} \right\rangle, \tag{14}$$

and

$$\Theta_{ij} \equiv \left\langle u_i''^{(f)} \frac{\partial \left(I_f 2\mu S_{kj}\right)}{\partial x_k} \right\rangle + \left\langle u_j''^{(f)} \frac{\partial \left(I_f 2\mu S_{ki}\right)}{\partial x_k} \right\rangle, \tag{15}$$

where S_{kj} is the rate-of-strain of the instantaneous velocity field and $p''^{(f)}$ is the fluid phase fluctuating pressure. The trace of these quantities are denoted $\Theta = \frac{1}{2}\Theta_{ii}$ and $\Pi = \frac{1}{2}\Pi_{ii}$, respectively.

At steady state, the Reynolds stress transport equation is essentially a balance between the generation of fluid–phase fluctuations by the interphase TKE transfer term $\left\langle u_i''^{(f)} M_j^{(f)} \right\rangle + \left\langle u_j''^{(f)} M_i^{(f)} \right\rangle$ and the Θ_{ij} term that contains viscous dissipation (the distinction between dissipation rate and the fluctuating velocity-viscous stress divergence correlation in two-phase flows is explained in Appendix). The relative magnitude of these terms in the TKE transport equation is quantified by taking the trace of (13), scaling the terms by Vk_{ref}/d_p, and computing their volume averages over the fully–developed region of the fixed bed ($2.5d_p < x < 12.8d_p$). The normalized, volume–averaged interphase TKE transfer term is compared with Θ in Table 3. The value reported for both the uniform and clustered cases represents the ensemble average over 4 MIS. In comparison, the convective term is $O(10^{-1})$, the transport of triple-velocity correlation is $O(10^{-3})$, the production term is zero,[2] and the fluctuating velocity–pressure gradient correlation Π is $O(10^{-2})$.

Based on our finding that the steady state TKE is determined by the balance between interphase TKE transfer and the dissipation rate, we seek to explain why the clustered configuration results in higher fluid–phase TKE than the uniform configuration. We plot normalized Θ as a function of x/d_p in Fig. 5 (the normalization factor Vk_{ref}/d_p is the same as in Table 3, where k_{ref} is the TKE in the

[2]This is true in the limit of infinite MIS. Note that the mean velocity is practically constant in the fully–developed region (cf. Fig. 3a).

Table 3 Magnitude of dominant terms—interphase TKE transfer $\left\langle u_i''^{(f)} M_i^{(f)} \right\rangle$ and fluctuating velocity–viscous stress divergence correlation Θ in the TKE transport equation

	Uniform	Clustered
$\left\langle u_i''^{(f)} M_i^{(f)} \right\rangle$	0.87	0.77
Θ	−0.77	−0.68

Each term is volume–averaged over the fully–developed region $2.5d_p < x < 12.8d_p$, normalized by Vk_{ref}/d_p, and averaged over 4 realizations

upstream homogeneous turbulence, d_p is the particle diameter and V is the mean slip velocity). The fluctuating velocity–viscous stress divergence correlation $\Theta(x)$ acts as an energy sink inside the fixed bed. Downstream of $x = 6d_p$, the magnitude of $\Theta(x)$ in the clustered particle configuration is smaller than that in the uniform particle configuration. The integral of $\Theta(x)$ from $x = 6d_p$ to $x = 11d_p$ in the clustered particle configuration is 34% less than that in the uniform case. Therefore, Θ from the uniform particle configuration dissipates more energy compared to the clustered particle configuration. The lower level of Θ in the clustered particle configuration

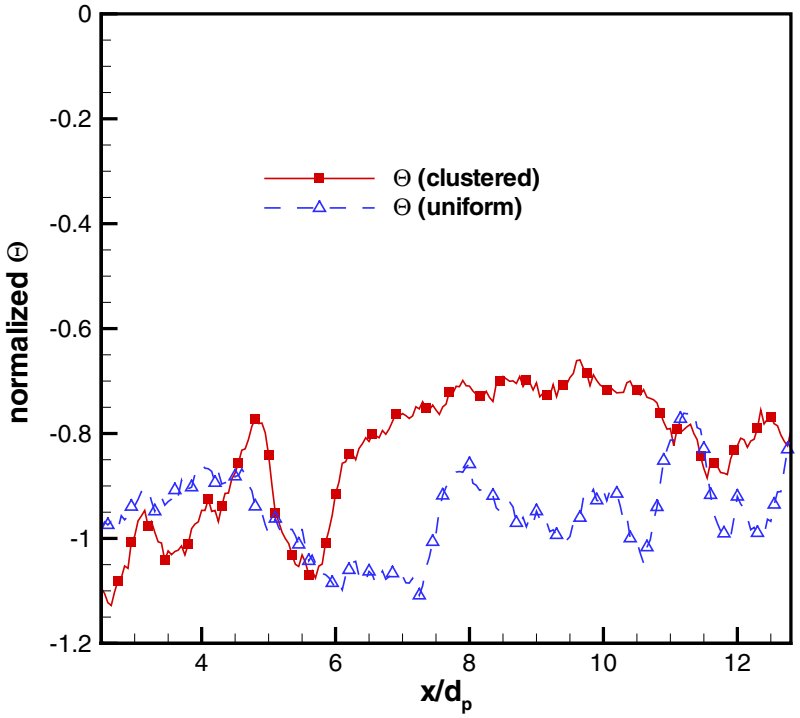

Fig. 5 The normalized half trace $\Theta = \Theta_{ii}/2$ of the fluctuating velocity–viscous stress divergence tensor inside the fixed bed for uniform particle configuration and clustered particle configuration. $\Theta(x)$ is normalized by Vk_{ref}/d_p, where k_{ref} is the TKE in the upstream homogeneous turbulence, d_p is the particle diameter and V is the mean slip velocity

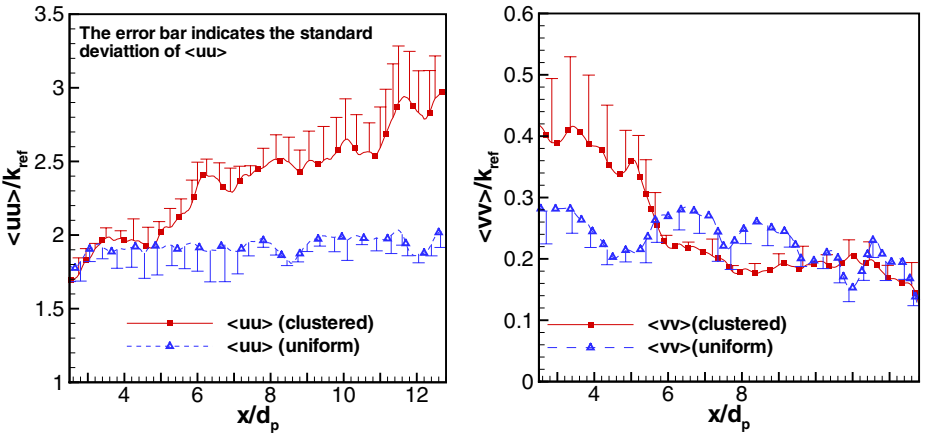

Fig. 6 Comparison of normalized $R_{11}^{(f)}(x_i)$ and $R_{22}^{(f)}(x_i)$ between uniform and clustered particle configurations. The *error bars* indicate the standard deviation

directly contributes to the higher level of fluid–phase TKE in the second half of the fixed bed ($6 < x/d_p < 12$) (cf. Fig. 4). Interphase TKE transfer is not plotted as a function of x/d_p in Fig. 5 because with only four independent realizations this surface–averaged quantity suffers from high statistical error. In general, it is difficult to reliably extract the spatial variation of surface–averaged statistics from such particle–resolved simulations, especially for dilute flows.

3.4 Anisotropy of the Reynolds stress

The variation of $R_{11}^{(f)}(x)$ and $R_{22}^{(f)}(x)$ in the fixed bed are shown in Fig. 6. Since $R_{33}^{(f)}$ is statistically identical to $R_{22}^{(f)}$, it is not shown here. The Reynolds stress becomes anisotropic inside the fixed bed and significant redistribution of Reynolds stress is observed for both uniform and clustered particle configurations. The magnitude of $R_{11}^{(f)}$ is higher than that of $R_{22}^{(f)}$ (or $R_{33}^{(f)}$) inside the fixed bed, even though the upstream turbulence is isotropic. To quantify the evolution of anisotropy of the Reynolds stress in the fixed bed, the invariants[3] ξ and η of the normalized Reynolds stress anisotropy tensor $b_{ij} = R_{ij}^{(f)}/(2k_f) - \frac{1}{3}\delta_{ij}$, at different x locations in the fixed bed are plotted in the ξ-η plane (see Fig. 7). The color of the symbols in Fig. 7 indicates the location in the fixed bed starting from $x = 2.5d_p$ (blue) to $x = 12.8d_p$ (red). Most of the symbols in Fig. 7, lie on the $\eta = \xi$ line, indicating an axisymmetric state of turbulence with one large eigenvalue. Therefore, the Reynolds-stress becomes increasingly more anisotropic as one moves along the streamwise direction in the fixed bed. There is not much difference in the Reynolds stress anisotropy between the uniform and clustered configurations.

[3]These are defined following Pope [49] as $6\xi^2 = b_{ij}b_{ij}$ and $6\eta^3 = b_{ij}b_{jk}b_{ki}$.

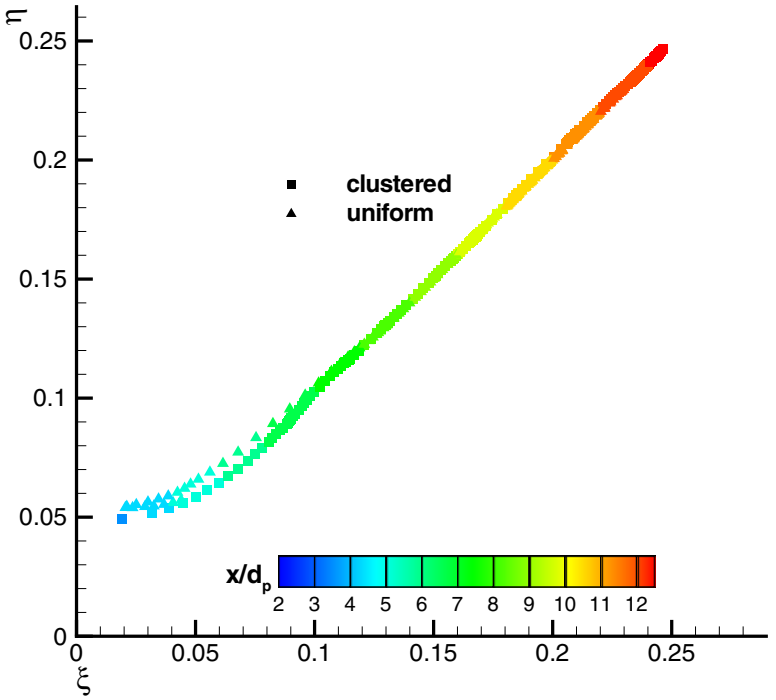

Fig. 7 The invariants ξ and η of the Reynolds stress anisotropy tensor. The *color* of the symbols indicates the location of the measurement going from $x = 2.5d_p$ (*blue*) at the inlet of the bed to $x = 12.8d_p$ (*red*) at the end of the bed. The Reynolds stress becomes progressively more anisotropic as we move deeper into the particle bed, starting from its initially isotropic state at the inlet

The reason why the Reynolds stress becomes anisotropic inside the fixed bed can be understood from the transport equation for the Reynolds stress. From the analysis in Section 3.2, the dominant terms on the right hand side of (13) are Θ_{ij} and the interphase TKE transfer term. We compute the invariants ξ and η of the normalized anisotropy tensors corresponding to the volume–average of Θ_{ij} and the interphase TKE transfer term $\left\langle u_i''^{(f)} M_j^{(f)} \right\rangle + \left\langle u_j''^{(f)} M_i^{(f)} \right\rangle$. Table 4 shows that both tensors are anisotropic. In single–phase turbulence it is reasonable to assume that the dissipation rate tensor is isotropic on the basis that dissipation arises from small scale motions that are locally isotropic. Often multiphase turbulence models use a modified single–phase model for the trace of the dissipation rate tensor. This result

Table 4 The invariants ξ and η of the normalized anisotropy tensors corresponding to the volume–average of Θ_{ij} and the interphase TKE transfer term $\left\langle u_i''^{(f)} M_j^{(f)} \right\rangle + \left\langle u_j''^{(f)} M_i^{(f)} \right\rangle$

	Particle configuration	ξ	η
Θ_{ij}	Uniform	0.2221	0.2178
	Clustered	0.2123	0.2123
Interphase TKE transfer	Uniform	0.3616	0.3630
	Clustered	0.3549	0.3562

shows that if particles are larger than the Kolmogorov scale, the assumption of an isotropic dissipation rate is not valid.

4 Discussion

The differences in TKE for varying levels of particle clustering that are found from these DNS results indicate that current multiphase turbulence models need to be extended to account for particle clustering effects. The dissipation of fluid–phase TKE depends on the level of particle clustering in these cases, indicating that models for the dissipation rate need to account for this effect. These DNS results also show that for particles larger than the Kolmogorov scale, the fluid–phase Reynolds stress tensor is anisotropic and modeling the fluid–phase TKE alone may not be adequate. Furthermore, the anisotropy of the dissipation rate is important in determining the anisotropic fluid–phase Reynolds stress. Multiphase turbulence models that are based on modified single-phase turbulence closures that assume an isotropic dissipation rate, and which do not account for particle clustering, will not be able to capture these effects.

However, including the effects of particle clustering in averaged two-fluid formulations is nontrivial because these formulations are incapable of representing particle clustering effects at their level of closure. Furthermore, the level of clustering changes with time because clustering is a dynamic phenomenon. It is also tightly coupled to the mean flow structure (that depends on the mean slip between the phases), the fluid (and particle) velocity fluctuations as well as inelasticity of collisions and particle-particle interactions that arise from cohesion or electrostatics.

While these DNS results provide interesting insights into multiphase turbulence physics and model development, they are preliminary results that need to be extended in several directions. These simulations were performed for static particle configurations because this allows us to characterize and maintain the pair–correlation statistic, but in a real flow the particle configuration will be dynamically changing in time. Therefore, allowing the particles to evolve freely in turbulent flow is one extension that is needed. If a statistically stationary clustered configuration is attained in these simulations, then time–averaging could be used to remove the limitation of relatively few independent simulations that resulted in wider confidence intervals in our ensemble–averaged estimates from fixed particle assemblies. A comprehensive exploration of the parameter space defined by the solid volume fraction, mean flow Reynolds number, turbulence Reynolds number, and particle size to Kolmogorov scale ratio is needed to fully characterize the interaction of particle clusters with turbulence.

It is also worth noting that the parameter range in the numerical and experimental studies can only be compared in a limited sense. In the CFB experiments [38] the Kolmogorov length scale is estimated to be $\eta = 146\mu$m, which is comparable to the particle length scale $d_p = 164\mu$m. The length scale of energy-containing eddies is estimated to be $l = 0.06$m, which is around 400 times the Kolmogorov length scale $\eta = 146\mu$m. The turbulent intensity is around 40%, and the turbulent Reynolds number $R_\lambda \approx 136$. In our DNS, the particle diameter d_p/η is 5.55 (cf. Table 1), and the turbulent Reynolds number $R_\lambda = 11.9$ is much smaller compared to the experiments. Hence, only the dissipation range of the energy spectrum is resolved

in this DNS study. The largest length and time scales in the experiments could not be simulated because the resolution requirement is too high and the computational cost is prohibitive. However, the key finding of this work is that these fluctuations are enhanced by the presence of inertial particles whose size is greater than the Kolmogorov scale. We note that the fluid velocity fluctuations induced in a laminar upstream flow by the presence of solid particles is quite significant for particles with high Stokes number. If the upstream turbulence level is lower than this level of velocity fluctuations induced by particles, then the presence of particles enhances turbulence (as is the case here). If the fully developed turbulent flow corresponds to a level of turbulence higher than this reference value, then one can expect different results (probably attenuation of turbulence). More definite conclusions can only be drawn if very large–scale simulations are performed.

5 Conclusions

Direct numerical simulations of turbulent flow past fixed particle assemblies are performed using a discrete–time, direct–forcing, immersed boundary method that imposes no–slip and no–penetration boundary conditions on each particle's surface. Motivated by experimental observations in fluidized beds, the effect of particle clustering on upstream turbulence is studied by comparing simulations past two different types of random particle configurations at the same solid volume fraction: (i) uniformly distributed particle configurations, and (ii) clustered particle configurations that result from a cooling granular gas simulation. Ensemble–averaged flow statistics are obtained from multiple independent simulations of statistically identical initial conditions for both the clustered and uniform cases for the same set of flow parameters: 5% solid volume fraction, mean flow Reynolds number $Re_p = 50$, Taylor–scale Reynolds number of upstream turbulence $R_\lambda = 11.9$, and particle size to Kolmogorov scale ratio $d_p/\eta = 5.5$. It is observed that the level of fluid–phase turbulent kinetic energy (TKE) is enhanced (compared to its upstream value) by the presence of particles in both configurations, and this is consistent with experimental observations. However, for the clustered cases the level of fluid–phase TKE is always greater than that of the uniform case at the same streamwise location. By isolating the effect of particle clustering from volume fraction, these DNS results demonstrate that particle clustering enhances turbulent velocity fluctuations in the fluid phase. The fluid–phase TKE dissipation rate reveals that a lower rate of dissipation in the clustered particle configurations directly contributes to the greater enhancement of fluid–phase TKE as compared to the uniform particle configurations. Starting from its reference upstream isotropic state at the beginning of the fixed bed, the fluid–phase Reynolds stress becomes increasingly anisotropic along the streamwise direction. In this problem, the fluid–phase Reynolds stress evolution is primarily determined by the balance between interphase transfer of TKE and viscous dissipation. The simulations reveal that the source of anisotropy in the Reynolds stress lies in the anisotropy of the interphase TKE transfer and dissipation tensors. The DNS results indicate that multiphase turbulence models should consider the effect of particle clusters and anisotropy in the dissipation model, and that they should also consider the evolution of the anisotropic Reynolds stress (not just the TKE).

Acknowledgements This work has been supported by National Energy Technology Laboratory, US Department of Energy grant number DE-AC02-07CH11358. The authors would also like to thank Dr. Jamal Mohd.-Yusof for sharing his base code for the hydrodynamic solver, and Dr. Madhusudan G. Pai for providing the clustered particle configurations from his granular cooling gas simulations.

Appendix: The Fluctuating Velocity-Viscous Stress Divergence Correlation in Two-phase Flows and the Dissipation Rate of Turbulence

The correlation between fluctuating velocity and the gradient of viscous stress (or rate-of-strain) in multiphase turbulence that is obtained from particle–resolved DNS in this work is different from the dissipation rate inferred from point–particle DNS as discussed in Xu and Subramaniam [66]. Here we clarify the difference between the fluctuating velocity-viscous stress divergence correlation Θ_{ij} (cf. (15)), and approximation of its trace by models for the dissipation rate of turbulence in particle–laden flow that are based on modifications to the dissipation model in single–phase turbulence. Specifically, we note that while the dissipation in single–phase turbulence is a square term that always results in a decrease of turbulent kinetic energy, the same property for the viscous part of Θ_{ij} is not proved.

The term corresponding to $\left\langle u_j^{\prime\prime(f)} \partial(I_f 2\mu S_{ki})/\partial x_k \right\rangle$ in single–phase turbulence is $2\nu \left\langle u_j \partial s_{ki}/\partial x_k \right\rangle$. The trace of this term simplifies as follows (see Eq. 5.163 in Pope [49])

$$2\nu \left\langle u_j \frac{\partial s_{kj}}{\partial x_k} \right\rangle = \nu \left\langle u_j \frac{\partial^2 u_j}{\partial x_k \partial x_k} \right\rangle = 2\nu \frac{\partial}{\partial x_j} \left\langle u_i s_{ij} \right\rangle - \varepsilon,$$

where $\varepsilon = 2\nu \left\langle s_{ij} s_{ij} \right\rangle$ is the dissipation rate in single–phase turbulence, which is a square term that always contributes to the decay of k. Therefore, in homogeneous single–phase turbulence the dissipation rate ε results in strictly decaying k according to the transport equation $dk/dt = -\varepsilon$. The correlation between fluctuating velocity and the gradient of viscous stress $\left\langle u_i^{\prime\prime(f)} \frac{\partial \left(I_f 2\mu S_{kj}\right)}{\partial x_k} \right\rangle$ in two-phase turbulence cannot be further decomposed as the sum of a square term in the strain rate and an additonal transport term as in single–phase turbulence theory due to the presence of the indicator function I_f in the derivative $\partial(\cdot)/\partial x_k$. So in statistically homogeneous flows the trace of Θ_{ij} is not guaranteed to be a square term that results in a strictly decaying k_f.

References

1. Ahmadi, G., Ma, D.: A thermodynamical formulation for dispersed multiphase turbulent flows: I. Basic theory. Int. J. Multiph. Flow **16**(2), 323–340 (1990)
2. Ahmadi, G., Ma, D.: A thermodynamical formulation for dispersed multiphase turbulent flows: II. Simple shear flows for dense mixtures. Int. J. Multiph. Flow **16**(2), 341–351 (1990)
3. Apte, S.V., Martin, M., Patankar, N.A.: A numerical method for fully resolved simulation (FRS) of rigid particle flow interactions in complex flows. J. Comput. Phys. **228**, 2712–2738 (2009)
4. Bagchi, P., Balachandar, S.: Effect of turbulence on the drag and lift of a particle. Phys. Fluids **15**(11), 3496–3513 (2003)
5. Bagchi, P., Balachandar, S.: Response of the wake of an isolated particle to an isotropic turbulent flow. J. Fluid Mech. **518**, 95–123 (2004)

6. Balzer, G., Boelle, A., Simonin, O.: Eulerian gas–solid flow modelling of dense fluidized bed. In: Fluidization VIII. International Symposium of Engineering Foundation, pp. 1125–1134 (1998)
7. Bhusarapu, S., Al Dahhan, M.H., Duduković, M.P.: Solids flow mapping in a gas–solid riser: mean holdup and velocity fields. Powder Technol. **163**(1–2), 98–123 (2006)
8. Bolio, E., Yasuna, J., Sinclair, J.: Dilute turbulent gas-solid flow in risers with particle-particle interactions. AIChE J. **41**(5), 1375–1388 (1995)
9. Bolio, E.J., Sinclair, J.L.: Gas turbulence modulation in the pneumatic conveying of massive particles in vertical tubes. Int. J. Multiph. Flow **21**(6), 985–1001 (1995)
10. Brereton, C.M.H., Grace, J.R.: Microstructural aspects of the behavior of circulating fluidized-beds. Chem. Eng. Sci. **48**(14), 2565–2572 (1993)
11. Burton, T.M., Eaton, J.K.: Fully resolved simulations of particle-turbulence interaction. J. Fluid Mech. **545**, 67–111 (2005)
12. Cocco, R., Shaffer, F., Hays, R., Reddy Karri, S.B., Knowlton, T.: Particle clusters in and above fluidized beds. Powder Technol. **203**(1), 3–11 (2010)
13. Drew, D.A., Passman, S.L.: Theory of multicomponent fluids. Applied mathematical sciences, vol. 135. Springer (1999)
14. Fan, M., Marshall, W., Daugaard, D., Brown, R.C.: Steam activation of chars produced from oat hulls and corn stover. Bioresour. Technol. **93**(1), 103–107 (2004)
15. Garg, R., Tenneti, S., Mohd.-Yusof, J., Subramaniam, S.: Direct numerical simulation of gas-solid flow based on the immersed boundary method. Engineering Science Reference, Ch. Computational Gas-Solids Flows and Reacting Systems: Theory, Methods and Practice (2009)
16. Glowinski, R., Pan, T., Helsa, T., Joseph, D.: A distributed Lagrange multiplier/fictitious domain method for particulate flows. Int. J. Multiph. Flow **25**(5), 755–794 (1999)
17. Glowinski, R., Pan, T.W., Helsa, T.I., Joseph, D.D., Periaux, J.: A fictitious domain approach to the direct numerical simulation of incompressible viscous flow past moving rigid bodies: application to particulate flow. J. Comput. Phys. **169**(2), 363–426 (2001)
18. Goldstein, D., Handler, R., Sirovich, L.: Modeling a no–slip flow boundary with an external force field. J. Comput. Phys. **105**(2), 354–366 (1993)
19. Gore, R.A., Crowe, C.T.: Effect of particle size on modulating turbulent intensity. Int. J. Multiph. Flow **15**(2), 279–285 (1989)
20. Grace, J., Tuot, J.: Theory for cluster formation in vertically conveyed suspensions of intermediate density. T. I. Chem. Eng.–Lond. **57**(1), 49–54 (1979)
21. Halvorsen, B., Guenther, C., O'Brien, T.J.: CFD calculations for scaling of a bubbling fluidized bed. In: Proceedings of the AIChE Annual Meeting, pp. 16–21. AIChE, San Francisco (2003)
22. Heynderickx, G.J., Das, A., De Wilde, J., Marin, G.: Effect of clustering on gas-solid drag in dilute two-phase flow. Ind. Eng. Chem. Res. **43**(16), 4635–4646 (2004)
23. Hill, R., Koch, D.L., Ladd, A.J.C.: The first effects of fluid inertia on flows in ordered and random arrays of spheres. J. Fluid Mech. **448**, 213–241 (2001)
24. Hill, R., Koch, D.L., Ladd, A.J.C.: Moderate-Reynolds-numbers flows in ordered and random arrays of spheres. J. Fluid Mech. **448**, 243–278 (2001)
25. Hu, H.H., Patankar, N.A., Zhu, M.Y.: Direct numerical simulations of fluid–solid systems using the arbitrary Lagrangian–Eulerian technique. J. Comput. Phys. **169**(2), 427–462 (2001)
26. Jackson, R.: The dynamics of fluidized particles. Cambridge Monographs on Mechanics. Cambridge University Press, Cambridge (2000)
27. Kim, D., Choi, H.: Immersed boundary method for flow around an arbitrarily moving body. J. Comput. Phys. **212**, 662–680 (2006)
28. Kim, J., Moin, P.: Application of a fractional-step method to incompressible Navier–Stokes equations. J. Comput. Phys. **59**, 308–323 (1985)
29. Knowlton, T., Karri, S., Issangya, A.: Scale-up of fluidized-bed hydrodynamics. Powder Technol. **150**, 72–77 (2005)
30. Krol, S.A.P., De Lasa, H.: Particle clustering in down flow reactors. Powder Technol. **108**(1), 6–20 (2000)
31. Ladd, A.J.C.: Simulations of particle-fluid suspensions with the Lattice–Boltzmann equation. In: Plenary Lecture at the Third M.I.T. Conference on Computational Fluid and Solid Mechanics. Cambridge, Massachusetts (2005)
32. Ladd, A.J.C., Verberg, R.: Lattice–Boltzmann simulations of particle-fluid suspensions. J. Stat. Phys. **104**, 119–1251 (2001)
33. Langford, J.A.: Toward Ideal Large-Eddy Simulation. Ph.D. thesis, University of Illinois at Urbana-Champaign, IL (2000)

34. Li, F.X., Fan, L.-S.: Clean coal conversion processes progress and challenges. Energy Environ. Sci. **1**, 248–267 (2008)
35. Lucci, F., Ferrante, A., Elghobashi, S.: Modulation of isotropic turbulence by particles of Taylor length-scale size. J. Fluid Mech. **650**, 5 (2010)
36. Mohd. Yusof, J.: Interaction of Massive Particles with Turbulence. Ph.D. thesis, Cornell University (1996)
37. Moran, J.C., Glicksman, L.R.: Experimental and numerical studies on the gas flow srrounding a single cluster applied to a circulating fluidized bed. Chem. Eng. Sci. **58**(9), 1879–1886 (2003)
38. Moran, J.C., Glicksman, L.R.: Mean and fluctuating gas phase velocities inside a circulating fluidized bed. Chem. Eng. Sci. **58**, 1867–1878 (2003)
39. Morinishi, Y., Lund, T.S., Vasilyev, O.V., Moin, P.: Fully conservative higher order finite difference schemes for incompressible flow. J. Comput. Phys. **142**, 1 (1998)
40. Nomura, T., Hughes, T.J.R.: An arbitrary Lagrangian–Eulerian finite element method for interaction of fluid and a rigid body. Comput. Methods Appl. Mech. Eng. **95**, 115 (1992)
41. O'Brien, T., Syamlal, M.: Particle cluster effects in the numerical simulation of a circulating fluidized bed. In: Fourth International Conference on Circulating Fluidized Beds. Somerset, PA (1993)
42. Pai, M.G., Subramaniam, S.: Second-order transport due to fluctuations in clustering particle systems. In: Proceedings of the 60th Annual Meeting of the Division of Fluid Dynamics. The American Physical Society. Salt Lake City, UT (2007)
43. Pai, M.G., Subramaniam, S.: A comprehensive probability density function formalism for multiphase flows. J. Fluid Mech. **628**, 181–228 (2009)
44. Patankar, N., Singh, P., Joseph, D., Glowinski, R., Pan, T.: A new formulation of the distributed Lagrange multiplier/fictitious domain method for particulate flows. Int. J. Multiph. Flow **26**(9), 1509–1524 (2000)
45. Peskin, C.S.: Flow patterns around heart valves: a numerical method. J. Comput. Phys. **25**, 220 (1977)
46. Peskin, C.S.: The immersed boundary method. Acta Numer. **11**, 479–517 (2002)
47. Pita, J., Sundaresan, S.: Gas-solid flow in vertical tubes. AIChE J. **37**(7), 1009–1018 (1991)
48. Pita, J., Sundaresan, S.: Developing flow of a gas-particle mixture in a vertical riser. AIChE J. **39**(4), 541–552 (1993)
49. Pope, S.: Turbulent Flows. Cambridge University Press (2000)
50. Prosperetti, A., Oguz, H.: PHYSALIS: a new o(N) method for the numerical simulation of disperse systems. Part I: potential flow of spheres. J. Comput. Phys **167**, 196–216 (2001)
51. Rogallo, R.S.: Numerical Experiments in Homogeneous Turbulence. Technical Report TM81315, NASA (1981)
52. Saw, E.W., Shaw, R.A., Ayyalasomayajula, S., Chuang, P.Y., Gylfason, A.: Inertial clustering of particles in high-Reynolds-number turbulence. Phys. Rev. Lett. **100**(21), 214501 (2008)
53. Sharma, N., Patankar, N.: A fast computation technique for the direct numerical simulation of rigid particulate flows. J. Comput. Phys. **205**(2), 439–457 (2005)
54. Sinclair, J., Jackson, R.: Gas-particle flow in a vertical pipe with particle-particle interactions. AIChE J. **35**, 1473–1486 (1989)
55. Stoyan, D., Kendall, W.S., Mecke, J.: Stochastic Geometry and Its Applications. Wiley, NY (1995)
56. Takagi, S., Oguz, H., Zhang, Z., Prosperetti, A.: PHYSALIS: a new method for particle simulation. Part II: two-dimensional Navier-stokes flow around cylinders. J. Comput. Phys. **187**, 371–390 (2003)
57. Ten Cate, A., Derksen, J.J., Portela, L.M., van den Akker, H.E.A.: Fully resolved simulations of colliding monodisperse spheres in forced isotropic turbulence. J. Fluid Mech. **519**, 233–271 (2004)
58. Tenneti, S., Garg, R., Hrenya, C.M., Fox, R.O., Subramaniam, S.: Direct numerical simulation of gas-solid suspensions at moderate Reynolds number: quantifying the coupling between hydrodynamic forces and particle velocity fluctuations. Powder Technol. **203**(1), 57–69 (2010)
59. Tsuji, Y., Morikawa, Y., Shiomi, H.: LDV measurements of an air-solid two-phase flow in a vertical pipe. J. Fluid Mech. **139**, 417–434 (1984)
60. Uhlmann, M.: An immersed boundary method with direct forcing for the simulation of particulate flows. J. Comput. Phys. **209**(2), 448–476 (2005)
61. Uhlmann, M.: Investigating turbulent particulate channel flow with interface-resolved DNS. In: 6th International Conference on Multiphase Flow ICMF 2007. Leipzig, Germany, 9–13 July 2007

62. van der Hoef, M.A., Beetstra, R., Kuipers, J.: Lattice–Boltzmann simulations of low-Reynolds-number flow past mono- and bidisperse arrays of spheres: results for the permeability and drag force. J. Fluid Mech. **528**, 233–254 (2005)
63. Vasilyev, O.V.: High order finite difference schemes on non-uniform meshes with good conservation properties. J. Comput. Phys. **157**, 746–761 (1999)
64. Wylie, J., Koch, D.L., Ladd, A.: Rheology of suspensions with high particle inertia and moderate fluid inertia. J. Fluid Mech. **480**, 95 (2003)
65. Xu, Y.: Modeling and direct numerical simulation of particle–laden turbulent flows. Ph.D. thesis, Iowa State Univ., Ames, IA (2008)
66. Xu, Y., Subramaniam, S.: Consistent modeling of interphase turbulent kinetic energy transfer in particle-laden turbulent flows. Phys. Fluids doi:10.1063/1.2756579 (2007)
67. Yang, N., Wang, W., Ge, W., Li, J.H.: CFD simulation of concurrent-up gas-solid flow in circulating fluidized beds with structure-dependent drag coefficient. Chem. Eng. J. **96**(1–3), 71–80 (2003)
68. Yin, X., Sundaresan, S.: Drag law for bidisperse gas-solid suspensions containing equally sized spheres. Ind. Eng. Chem. Res. **48**(1), 227–241 (2008)
69. Zhang, Z., Prosperetti, A.: A method for particle simulations. J. Appl. Mech. **70**, 64–74 (2003)
70. Zhang, Z., Prosperetti, A.: A second-order method for three-dimensional particle flow simulations. J. Comput. Phys **210**, 292–324 (2005)
71. Zhang, M., Qian, Z., Yu, H., Wei, F.: The solid flow structure in a circulating fluidized bed riser/downer of 0.42-m diameter. Powder Technol. **129**(1–3), 46–52 (2003)